APL Materials

RESEARCH ARTICLE | NOVEMBER 20 2023

Energy levels of carbon dangling-bond center (P_{bC} center) at 4H-SiC(0001)/SiO_2 interface

Mitsuru Sometani; Yusuke Nishiya; Ren Kondo; Rei Inohana; Hongyu Zeng; Hirohisa Hirai; Dai Okamoto; Yu-ichiro Matsushita; Takahide Umeda

Check for updates

APL Mater. 11, 111119 (2023)
https://doi.org/10.1063/5.0171143

CrossMark

21 November 2023 05:56:40

AIP Publishing

AMERICAN ELEMENTS
THE ADVANCED MATERIALS MANUFACTURER
The Next Generation of Material Science Catalogs
Now Invent.
www.americanelements.com

Energy levels of carbon dangling-bond center (P_{bC} center) at 4H-SiC(0001)/SiO_2 interface

Cite as: APL Mater. 11, 111119 (2023); doi: 10.1063/5.0171143
Submitted: 7 August 2023 • Accepted: 27 October 2023 •
Published Online: 20 November 2023

Mitsuru Sometani,[1,a)] Yusuke Nishiya,[2] Ren Kondo,[3] Rei Inohana,[3] Hongyu Zeng,[3] Hirohisa Hirai,[1] Dai Okamoto,[3] Yu-ichiro Matsushita,[2,4] and Takahide Umeda[3]

AFFILIATIONS

[1] Advanced Power Electronics Research Center, National Institute of Advanced Industrial Science and Technology, 16-1 Onogawa, Tsukuba, Ibaraki 305-8569, Japan
[2] Institute for Innovative Research, Tokyo Institute of Technology, 2-12-1 Ookayama, Meguro-ku, Tokyo 152-8550, Japan
[3] Graduate School of Pure and Applied Sciences, University of Tsukuba, 1-1-1 Tennodai, Tsukuba, Ibaraki 305-8577, Japan
[4] Quantum Material and Applications Research Center, National Institutes for Quantum Science and Technology, 2-12-1, Ookayama, Meguro-ku, Tokyo 152-8552, Japan

[a)] **Author to whom correspondence should be addressed:** m.sometani@aist.go.jp

ABSTRACT

The electric properties of the carbon dangling-bond (P_{bC}) center at a thermally oxidized 4H-SiC(0001)/SiO_2 interface are investigated. We experimentally and theoretically determine the energy levels of the associated interface states to estimate the impacts of the P_{bC} center on power device operations. By combining electrically detected magnetic resonance spectroscopy and capacitance–voltage measurements, the two P_{bC} electronic levels [(0/−) and (+/0)] are determined as ~1.2 and 0.6 eV from the valence band maximum, respectively. The effective correlation energy of the P_{bC} center is 0.6 eV, which is 1.5 times larger than that of the silicon dangling-bond (P_b) center at Si/SiO_2 interfaces. Our first-principles calculations confirm that the electronic levels of P_{bC} are similar to experimental values. Considering these energy levels, the P_{bC} center must impact both p- and n-channel devices, which is closely related to previously reported channel features.

© 2023 Author(s). All article content, except where otherwise noted, is licensed under a Creative Commons Attribution (CC BY) license (http://creativecommons.org/licenses/by/4.0/). https://doi.org/10.1063/5.0171143

21 November 2023 05:56:40

The 4H polytype of silicon carbide (SiC) has attracted considerable interest in high-voltage and high-temperature power devices due to its wide bandgap, high breakdown electric field, and high thermal conductivity.[1,2] SiC is preferred over other wide-bandgap semiconductors when fabricating metal–oxide–semiconductor (MOS) devices due to its ability to form thermally grown SiO_2 as a gate oxide film.[3–5] Although SiC-based MOS field-effect transistors (FETs) have become commercially available in recent years, their on-resistance is still much higher than expected,[2,6,7] which is caused by the low field-effect mobility (μ_{FE}) in n-MOS. One reason for the decrease in μ_{FE} is the inversion charge trapping by interface defects, resulting in a decreased mobile carrier density in the channel.[8–11] Furthermore, the threshold voltage (V_{th}) varies from its ideal value due to fewer mobile carriers.[12] Although various defect structures have been suggested at the 4H-SiC(0001)/SiO_2 interface, such as carbon dimers,[13] details of the microscopic origins are unclear. Electron-spin-resonance (ESR) and electrically detected-magnetic-resonance (EDMR) spectroscopy are powerful tools for identifying the microscopic origins of such interface defects.[14–18]

We previously reported ESR observations of carbon-related paramagnetic defects at the 4H-SiC(0001)/SiO_2 interface, called the P_{bC} center. The P_{bC} center is a carbon version of the well-known P_b center.[19,20] The P_b center belongs to the family of Si dangling bonds (DBs) intrinsically formed at Si/SiO_2 interfaces. In the Si-MOS system, the P_b center is one of the primary interface defects. Thus, it is also considered the primary interface defect in the SiC-MOS system. A reduced P_{bC} center density was evaluated by ESR to closely correlate with μ_{FE} improvements in n-MOS when employing modified oxidation processes, such as NO post oxidation annealing (POA), $POCl_3$ POA, and ultra-high-temperature (UHT) oxidation processes.[21–25] Our study uses EDMR and first-principles calculations to reveal that the P_{bC} center consists of a carbon adatom on the 4H-SiC(0001) honeycomb-like structure.[26]

© Author(s) 2023

Another important insight obtained by EDMR is that the P_{bC} center signal is strong when applying a certain negative gate voltage (V_g). Thus, a high density of interface states near the valence band maximum is the primary product of the P_{bC} center. This suggests that the P_{bC} center should have a minor impact on n-MOS characteristics. To identify the relationship between the MOS characteristics and P_{bC} center, it is essential to quantitatively estimate the energy level. It has been reported that the combination of ESR and capacitance–voltage ($C - V$) measurements accurately evaluates the defect levels in Si MOS systems.[27] This paper develops an analytical method to apply their combination for 4H-SiC MOS systems to determine the energy level of the interface states caused by the P_{bC} center.

For the highly sensitive EDMR measurements, we prepared n-channel lateral 4H-SiC MOSFETs with wide dimensions (gate length/width = 5/2000 μm) on a 4° off-cut Al-doped p-type 4H-SiC(0001) epitaxial layer ($N_A - N_D = 3 \times 10^{15}$ cm^{-3}). The source/drain regions were formed via P ion implantation, and the body region was formed using Al ion implantation, both at 600 °C. This process was followed by activation annealing at 1650 °C for 5 min under an Ar atmosphere with a carbon capping layer.[28] After removing the carbon capping layer, the surface was cleaned using RCA cleaning, followed by sacrificial oxidation and hydrofluoric acid (HF) dipping. Thermal oxidation at 1200 °C provided a 30-nm thick gate oxide using dry O_2. After thermal oxidation, post-oxidation annealing was conducted at 1200 °C under an argon atmosphere for 30 min. Next, chemical vapor deposition (CVD) deposited n-type polycrystalline Si, which was patterned using photolithography techniques to form the gate electrodes. The source/drain and body contacts were formed by depositing Al and Ni stacks, followed by annealing at 900 °C under an N_2 atmosphere.

We conducted bipolar amplification-effect (BAE) EDMR measurements using this sample to amplify the EDMR signals of interface defects.[29] In this regime, we biased a constant current (I_d) from the drain to the body and monitored the ESR-induced current changes in the drain–source current (I_{EDMR}), as shown in Fig. 1(a). We used the standard lock-in amplification technique synchronized to magnetic-field modulations at 1.56 kHz.[15,23] The ESR transitions were excited by a 200-mW 9.45 GHz microwave at room temperature (297 K). We also investigated the $C - V$ characteristics of a MOS capacitor fabricated on the same p-type epitaxial layers. The frequency of the $C - V$ measurements was 5 Hz. Figure 1(b) shows the typical EDMR spectra of the Si-face 4H-SiC MOSFET. The single strong EDMR peak is attributed to the P_{bC} center (electron spin of $S = 1/2$). We believe that the origin of the EDMR signal is the same as for the ESR signal (spin density of 3–4 × 10^{12} cm^{-2}) observed for as-oxidized 4H-SiC(0001) epitaxial layers under similar conditions.[16,25]

Figure 2 shows the gate-bias dependencies of the EDMR signals. The V_g was swept toward the negative direction, changing the Fermi energy of SiC at the interface (E_f) from the mid-gap to the valence band maximum. The EDMR signal intensity (ΔI) increases at $V_g = -3$ V and decreases at $V_g = -10$ V for all I_d conditions. This indicates that the spin state of the P_{bC} center changes from doubly occupied ($S = 0$) to singly occupied ($S = 1/2$) at $V_g = -3$ V and then changes to the empty state ($S = 0$) at $V_g = -10$ V. These voltages reflect the electric properties of the P_{bC} center. When V_g less than −10 V is applied, a small ΔI is observed. This signal does not show hyperfine structures due to the P_{bC} center, suggesting it originated from other minor structures.[30] I_{EDMR} in the figure is used to normalize the signals.

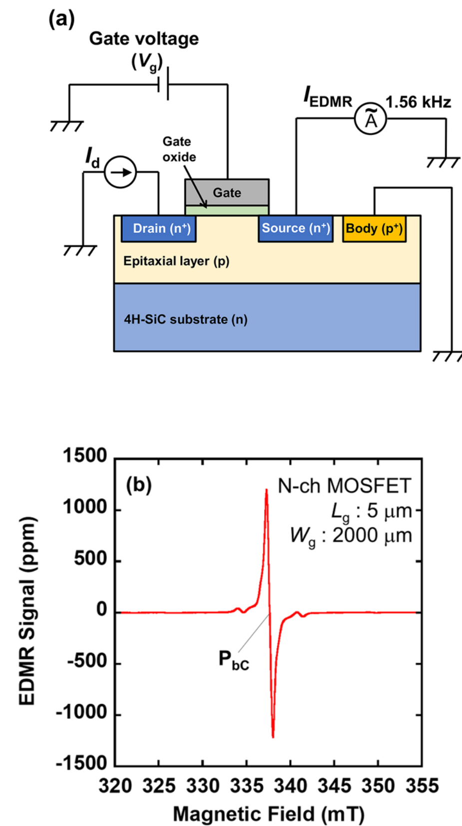

FIG. 1. (a) Schematic cross-section of n-channel lateral 4H–SiC MOSFETs with a wide dimension (gate length/width = 5/2000 μm) for highly sensitive EDMR measurements and the BAE EDMR setup. (b) Typical EDMR spectra show only one strong EDMR peak attributed to the P_{bC} center (electron spin of $S = 1/2$).

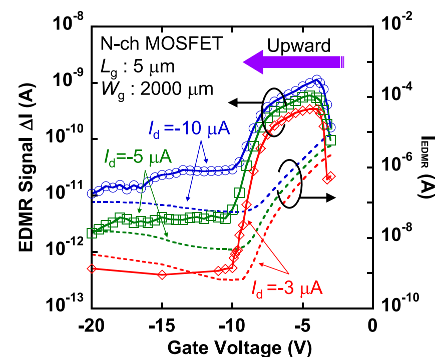

FIG. 2. Variations in the EDMR signals and I_{EDMR} at various I_d and V_g. The I_d was −3, −5, −10 μA, and the upward V_g was swept from −3 to −20 V.

21 November 2023 05:56:40

© Author(s) 2023

We then measured the $C-V$ characteristics to estimate E_f during the upward V_g sweep. To estimate the relationship between the capacitance and E_f, the surface potential (ψ_s) is calculated from the low-frequency capacitance (C_{LF}) and oxide capacitance (C_{OX}) as

$$\psi_s(V_g) = \int(1 - C_{LF}/C_{OX})dV_g + A, \quad (1)$$

where A is an integration constant.[31,32] The flat-band capacitance (C_{FB}) and flat-band voltage (V_{FB}) are used to determine A. Figure 3(a) shows the $C-V$ characteristics of a fresh MOS capacitor fabricated on the same chip as the MOSFET for the EDMR measurements. The $C-V$ characteristic in the upward measurement showed stretching due to charge trapping at various interface traps and/or near interface traps (NIT).[33] The unusual shape of the $C-V$ curve on the upward V_g sweep makes it difficult to accurately determine the C_{FB} and V_{FB}. To reliably estimate E_f at V_g, the impact of hole traps on the $C-V$ characteristics should be carefully considered. Associated with the high density of interface defects, there is a trade-off between the observations of strong EDMR signals and distortion in the $C-V$ characteristics, prohibiting accurate E_f estimations.

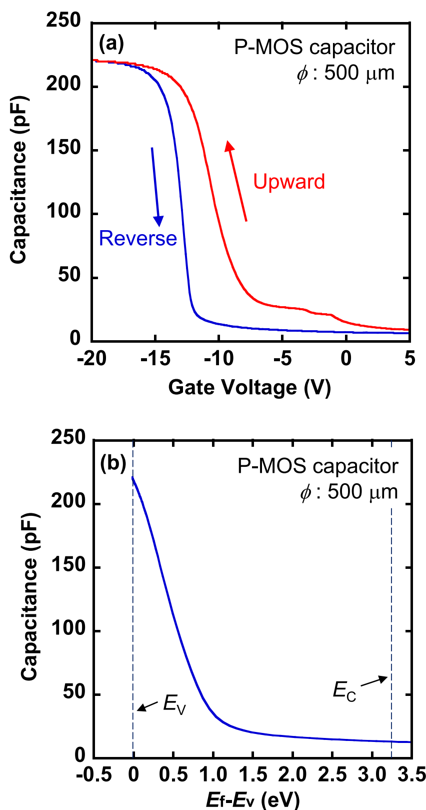

FIG. 3. (a) Upward and reverse side $C-V$ characteristics of a fresh p-MOS capacitor fabricated on the same chip as the n-MOSFET for the EDMR measurements. (b) Relationship between the capacitance and E_f estimated from the reverse side $C-V$ characteristics using the $C-\psi_s$ method.

To minimize E_f estimation errors due to interface defects, we note that the reverse V_g sweep shows little stretching. The difference in the curves between the sweep directions is attributed to hole traps, which are easily filled during the upward V_g sweep and kept filled during the reverse sweep because the de-trapping time is longer than the $C-V$ measurement duration. The relationship between the capacitance and E_f of the MOS is less affected by filled traps. We determined the E_f from the reverse sweep $C-V$ characteristics.

The $C-\psi_s$ method has been proposed to evaluate the accuracy of the ψ_s at the SiC-MOS interface with a large density of interface traps (D_{it}).[34,35] In this method, the integration constant A in Eq. (1) is determined from the linear relationship between the depletion capacitance (C_{dep}) and ψ_s, while C_{FB} and V_{FB} are not required. Using C_{dep} in the analysis cancels the effect of interface traps. Figure 3(b) shows the relationship between the MOS capacitance and E_f estimated from the reverse side $C-V$ characteristics using the $C-\psi_s$ method. Assuming that the relationship between C_{dep} and ψ_s is identical irrespective of the sweep direction allows estimating E_f at a given V_g for the upward sweep using the relationship in Fig. 3(b).

V_g in Fig. 2 is then converted into E_f to give Fig. 4. Here, the normalized signals, $\Delta I/I_{EDMR}$, were employed for the vertical axis. The EDMR signals were observed for V_g from −3 to −10 V during the upward sweep. E_f in this voltage region shifts from ~1.2 to 0.6 eV from the valence band maximum of the 4H-SiC(0001) at the interface. This means that the (0/−) and (+/0) levels of the P_{bC} center are ~1.2 and 0.6 eV from the valence band maximum (E_v), respectively. Therefore, the effective correlation energy (U_{eff}) is derived from the difference between the doubly occupied level [(0/−) level] and the singly occupied level [(+/0) level] and is estimated as 0.6 eV for the P_{bC} center. This energy value is 1.5 times larger than that for P_b center in Si-MOS systems (~0.4 eV).[36] As spin localizations for both the P_{bC} center and P_b center are ~80% on each dangling-bond site,[20,26] the larger U_{eff} of P_{bC} is ascribed primarily to the smaller spatial extension of carbon atomic orbitals, causing greater Coulomb repulsion for the (0/−) level of the P_{bC} center.

We also performed first-principles calculations based on density functional theory for the (0/−) level of the P_{bC} center using

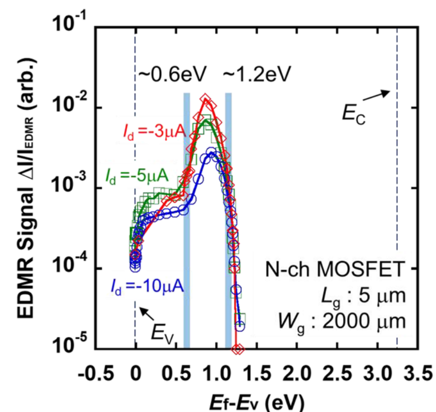

FIG. 4. EDMR signals at various E_f from the valence band maximum of the 4H-SiC(0001) interface.

21 November 2023 05:56:40

© Author(s) 2023

RSDFT[37,38] with norm-conserving pseudopotentials generated by the Troullier–Martins scheme. Our calculation model includes 170 atoms H-terminated in the 4H-SiC(0001)/SiO_2 interface with a single P_{bC} center. The single k-point (Γ point) is sampled, and spin-polarization is considered. The 80 × 80 × 180 real-space grids corresponding to 1.3×10^3 eV are adopted in the hexagonal unit cell where a = 12.38 Å and c = 30.38 Å. The lattice parameters are set at the values from previous research.[39,40] The atom positions in the simulation cell are optimized using the Perdew–Burke–Ernzerhof functional (PBE)[41] until the remaining forces go below 5×10^{-4} hartree/bohr.

To examine the in-gap state generated by the dangling bond of the C adatom, the calculations with the Heyd–Scuseria–Ernzerhof hybrid functional (HSE06)[42] for the structure obtained by PBE followed as HSE06 reproduces the experimental bandgap of SiC. The calculated bandgap of perfect 4H-SiC bulk is 3.21 eV, while the experimental bandgap is 3.26 eV at RT.[43] The results Fig. 5 suggest that the greatest occupied level in the negatively charged system by adding an extra electron is 1.24 eV above the valence band maximum. Visualization of the crystal structure and wave function was performed in VESTA.[44] The C adatom is chemically bonded with the three underlying Si atoms in the SiC substrate, with one dangling bond perpendicular to the substrate. The wave function of this in-gap state is the dangling bond of the adatom with a primarily p-like characteristic. The level is occupied by both up and down spins. Spin-polarization does not occur in the negatively charged system, while the $S = 1/2$ state is realized in a neutral system. These results agree well with the experimental fact that the EDMR signal loses intensity when E_f reaches E_v + 1.2 eV. This study is the first case that determines both the microscopic structure and energy levels of an interface defect for wide bandgap semiconductor MOS interfaces.

The estimated levels of the P_{bC} center affect both n- and p-MOSFET characteristics. This study demonstrates that the P_{bC} centers act as bipolar trap levels [(0/−) and (+/0) levels] for both electrons and holes. This indicates that P_{bC} centers can vary the V_{th} from its ideal value by reducing the mobile carriers in both the p- and n-channel MOSFETs. Suppressing the V_{th} deviation by NO POA or UHT oxidation processes[5,12,45] could be due to eliminating these levels. The wet oxidation process also effectively suppresses V_{th} deviations in the p-channel MOSFETs via hydrogen termination of the P_{bC} center.[46] In n-channel MOSFETs, there is a correlation between the reduced P_{bC} center density and μ_{FE} improvements for n-channel MOSFETs.[25] However, the P_{bC} center should not directly decrease the mobile electron density for n-channel MOSFETs as it generates levels near the valence band maximum. Furthermore, it has been reported that electrons trapped by interface states should have minor impacts on electron scattering.[7,47] These results suggest that the correlation of the P_{bC} center density and μ_{FE} is attributed to other interface states near the conduction band edge minimum rather than the P_{bC} center itself. It is speculated that the other interface state density is related to the density of the P_{bC} center. The next challenge is to reveal the origins of the P_{bC}-center-related defects in n-MOSFET devices.

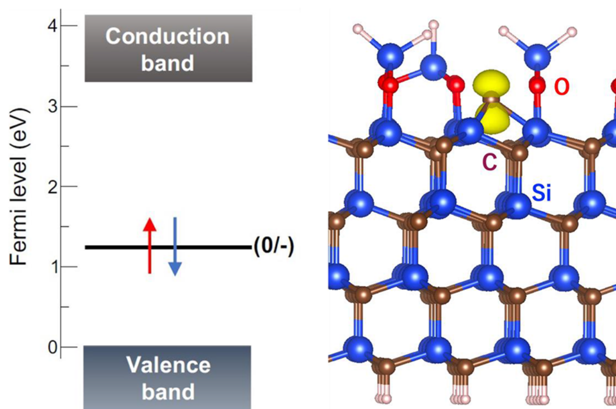

FIG. 5. Energy level diagram of the negatively charged 4H-SiC system with a P_{bC} center, and the calculated structural model at a SiC/SiO_2 interface. The calculated squared wave function of the highest occupied level is drawn with the isosurface for 15% of the maximum amplitude, where the small white balls depict H atoms that terminate the dangling bonds in the SiO_2 film. The crystal structure and wave function are visualized using VESTA.

In summary, we evaluated the energy levels of the P_{bC} center through the combination of EDMR and $C - V$ measurements. It was confirmed that the P_{bC} center energy level is within the 4H-SiC bandgap. Thus, it is considered one of the major active interface states. The (0/−) and (+/0) levels of the P_{bC} center are ~1.2 and 0.6 eV from the valence band maximum, respectively. The validity of the (0/−) level of the P_{bC} was confirmed by first-principles calculations. The levels of the P_{bC} center should reduce the mobile carrier density, resulting in V_{th} deviating from ideal for p- and n-channel MOSFETs. Considering the energy levels of the P_{bC} center, it has minor impacts on the n-MOSFET channel mobility. The relationship between the P_{bC} center elimination and μ_{FE} enhancement in n-MOSFETs is attributed to different defect types, whose densities are related to the density of the P_{bC} center. Further reductions to the P_{bC} center density and related defects are key to improving the SiC-MOS device performance.

This work was supported by JSPS KAKENHI (Grant Nos. JP20H00340 and JP21H04553) and MEXT as "Program for Promoting Researches on the Supercomputer Fugaku" (Grant No. JP-MXP1020200205).

The computation in this work has been done using (supercomputer Fugaku provided by the RIKEN Center for Computational Science/Supercomputer Center at the Institute for Solid State Physics at the University of Tokyo).

AUTHOR DECLARATIONS

Conflict of Interest

The authors have no conflicts to disclose.

Author Contributions

Mitsuru Sometani: Conceptualization (equal); Formal analysis (equal); Funding acquisition (equal); Investigation (equal); Writing – original draft (equal). **Yusuke Nishiya**: Formal analysis (equal); Investigation (equal); Writing – original draft (equal).

21 November 2023 05:56:40

© Author(s) 2023

Ren Kondo: Formal analysis (equal). **Rei Inohana**: Formal analysis (equal). **Hongyu Zeng**: Formal analysis (equal). **Hirohisa Hirai**: Investigation (equal); Writing – review & editing (equal). **Dai Okamoto**: Investigation (equal); Writing – review & editing (equal). **Yu-ichiro Matsushita**: Conceptualization (equal); Funding acquisition (equal). **Takahide Umeda**: Conceptualization (equal); Formal analysis (equal); Funding acquisition (equal); Writing – review & editing (equal).

DATA AVAILABILITY

The data that support the findings of this study are available within the article.

REFERENCES

[1] H. Matsunami, Jpn. J. Appl. Phys. **43**, 6835 (2004).
[2] T. Kimoto, Jpn. J. Appl. Phys. **54**, 040103 (2015).
[3] S. Harada, M. Okamoto, T. Yatsuo, K. Adachi, K. Fukuda, and K. Arai, IEEE Electron Device Lett. **25**, 292 (2004).
[4] A. Koyama, Y. Kiuchi, T. Mizushima, K. Takenaka, S. Matsunaga, M. Sometani, K. Nakayama, H. Ishimori, A. Kimoto, M. Takei, T. Kato, Y. Yonezawa, and H. Okumura, Mater. Sci. Forum **1004**, 899 (2020).
[5] K. Moges, T. Hosoi, T. Shimura, and H. Watanabe, Appl. Phys. Express **14**, 091006 (2021).
[6] T. Kimoto and H. Watanabe, Appl. Phys. Express **13**, 120101 (2020).
[7] M. Sometani, T. Hosoi, H. Hirai, T. Hatakeyama, S. Harada, H. Yano, T. Shimura, H. Watanabe, Y. Yonezawa, and H. Okumura, Appl. Phys. Lett. **115**, 132102 (2019).
[8] S. Harada, R. Kosugi, J. Senzaki, W. Cho, K. Fukuda, K. Arai, and S. Suzuki, J. Appl. Phys. **91**, 1568 (2002).
[9] T. Hatakeyama, Y. Kiuchi, M. Sometani, S. Harada, D. Okamoto, H. Yano, Y. Yonezawa, and H. Okumura, Appl. Phys. Express **10**, 046601 (2017).
[10] T. Hatakeyama, T. Masuda, M. Sometani, S. Harada, D. Okamoto, H. Yano, Y. Yonezawa, and H. Okumura, Appl. Phys. Express **12**, 021003 (2019).
[11] H. Yoshioka, J. Senzaki, A. Shimozato, Y. Tanaka, and H. Okumura, AIP Adv. **8**, 045217 (2018).
[12] P. Fiorenza, C. Bongiorno, F. Giannazzo, M. Alessandrino, A. Messina, M. Saggio, and F. Roccaforte, Appl. Surf. Sci. **557**, 149752 (2021).
[13] P. Fiorenza, F. Iucolano, G. Nicotra, C. Bongiorno, I. Deretzis, A. La Magna, F. Giannazzo, M. Saggio, C. Spinella, and F. Roccaforte, Nanotechnology **29**, 395702 (2018).
[14] T. Umeda, K. Esaki, R. Kosugi, K. Fukuda, T. Ohshima, N. Morishita, and J. Isoya, Appl. Phys. Lett. **99**, 142105 (2011).
[15] T. Umeda, G.-W. Kim, T. Okuda, M. Sometani, T. Kimoto, and S. Harada, Appl. Phys. Lett. **113**, 061605 (2018).
[16] T. Umeda, Y. Kagoyama, K. Tomita, Y. Abe, M. Sometani, M. Okamoto, S. Harada, and T. Hatakeyama, Appl. Phys. Lett. **115**, 151602 (2019).
[17] E. Higa, M. Sometani, H. Hirai, H. Yano, S. Harada, and T. Umeda, Appl. Phys. Lett. **116**, 171602 (2020).
[18] Y. Abe, A. Chaen, M. Sometani, S. Harada, Y. Yamazaki, T. Ohshima, and T. Umeda, Appl. Phys. Lett. **120**, 064001 (2022).
[19] Y. Nishi, Jpn. J. Appl. Phys. **10**, 52 (1971).
[20] K. L. Brower, Appl. Phys. Lett. **43**, 1111 (1983).
[21] G. Y. Chung, C. C. Tin, J. R. Williams, K. McDonald, R. K. Chanana, R. A. Weller, S. Pantelides, L. Feldman, O. Holland, M. Das, J. Palmour, and J. W. Palmour, IEEE Electron Device Lett. **22**, 176 (2001).
[22] D. Okamoto, M. Sometani, S. Harada, R. Kosugi, Y. Yonezawa, and H. Yano, IEEE Electron Device Lett. **35**, 1176 (2014).
[23] M. Sometani, D. Nagai, Y. Katsu, T. Hosoi, T. Shimura, M. Takei, Y. Yonezawa, and H. Watanabe, Jpn. J. Appl. Phys. **56**, 04CR04 (2017).
[24] T. Hosoi, Y. Katsu, K. Moges, D. Nagai, M. Sometani, H. Tsuji, T. Shimura, and H. Watanabe, Appl. Phys. Express **11**, 091301 (2018).
[25] T. Umeda, Y. Nakano, E. Higa, T. Okuda, T. Kimoto, T. Hosoi, H. Watanabe, M. Sometani, and S. Harada, J. Appl. Phys. **127**, 145301 (2020).
[26] T. Umeda, T. Kobayashi, M. Sometani, H. Yano, Y. Matsushita, and S. Harada, Appl. Phys. Lett. **116**, 071604 (2020).
[27] E. H. Poindexter, G. J. Gerardi, M. E. Rueckel, P. J. Caplan, N. M. Johnson, and D. K. Biegelsen, J. Appl. Phys. **56**, 2844 (1984).
[28] Y. Negoro, K. Katsumoto, T. Kimoto, and H. Matsunami, J. Appl. Phys. **96**, 224 (2004).
[29] T. Aichinger and P. M. Lenahan, Appl. Phys. Lett. **101**, 083504 (2012).
[30] This minor signal (intensities are two orders of magnitude smaller than the P_{bC} intensity) is nearly isotropic at the g factor of 2.002, suggesting it arises from another carbon-related interface defect. Judging from its dependence, the energy levels are supposedly in a shallower range in the valence-band side than for P_{bC}. Similar EDMR signals were found in nitrided a-face and m-face 4H-SiC MOSFETs (Ref. 17), implying its origin may be independent of 4H-SiC faces. No other EDMR signals were detected under other ranges (e.g., positive V_g) or wider magnetic field range (10–800 mT). Also, no bulk ESR centers or implantation damage (such as vacancy-type defects) were detected within our EDMR search.
[31] E. H. Nicollian and J. R. Brews, *MOS Physics and Technology* (Wiley, New York, 1982).
[32] D. K. Schroder, *Semiconductor Material and Device Characterization*, 3rd ed. (Wiley, Hoboken, NJ, 2006).
[33] Y. Karamoto, X. Zhang, D. Okamoto, M. Sometani, T. Hatakeyama, S. Harada, N. Iwamuro, and H. Yano, Jpn. J. Appl. Phys. **57**, 06KA06 (2018).
[34] H. Yoshioka, T. Nakamura, and T. Kimoto, J. Appl. Phys. **111**, 014502 (2012).
[35] H. Yoshioka, T. Nakamura, and T. Kimoto, J. Appl. Phys. **112**, 024520 (2012).
[36] J. E. Northrup, Phys. Rev. B **40**, 5875 (1989).
[37] J.-I. Iwata, D. Takahashi, A. Oshiyama, T. Boku, K. Shiraishi, S. Okada, and K. Yabana, J. Comput. Phys. **229**, 2339 (2010).
[38] Y. Hasegawa, J.-I. Iwata, M. Tsuji, D. Takahashi, A. Oshiyama, K. Minami, T. Boku, H. Inoue, Y. Kitazawa, I. Miyoshi, and M. Yokokawa, Int. J. High Perform. Comput. Appl. **28**, 335 (2014).
[39] T. Kobayashi, K. Harada, Y. Kumagai, F. Oba, and Y. Matsushita, J. Appl. Phys. **125**, 125701 (2019).
[40] T. Kobayashi and Y. Matsushita, J. Appl. Phys. **126**, 145302 (2019).
[41] P. Perdew, K. Burke, and M. Ernzerhof, Phys. Rev. Lett. **77**, 3865 (1996).
[42] J. Heyd, G. E. Scuseria, and M. Ernzerhof, J. Chem. Phys. **118**, 8207 (2003); Erratum **124**, 219906 (2006).
[43] T. Kimoto and J. A. Cooper, *Fundamentals of Silicon Carbide Technology* (Wiley, Singapore, 2014).
[44] K. Momma and F. Izumi, J. Appl. Cryst. **44**, 1272 (2011).
[45] K. Tachiki and T. Kimoto, IEEE Trans. Electron Devices **68**, 638 (2021).
[46] S. Katakami, H. Fujisawa, K. Takenaka, H. Ishimori, S. Takasu, M. Okamoto, M. Arai, Y. Yonezawa, and K. Fukuda, Mater. Sci. Forum **740–742**, 958 (2013).
[47] M. Noguchi, T. Iwamatsu, H. Amishiro, H. Watanabe, K. Kita, and N. Miura, Jpn. J. Appl. Phys. **58**, SBBD14 (2019).

21 November 2023 05:56:40

© Author(s) 2023